Nanoscale

Accepted Manuscript

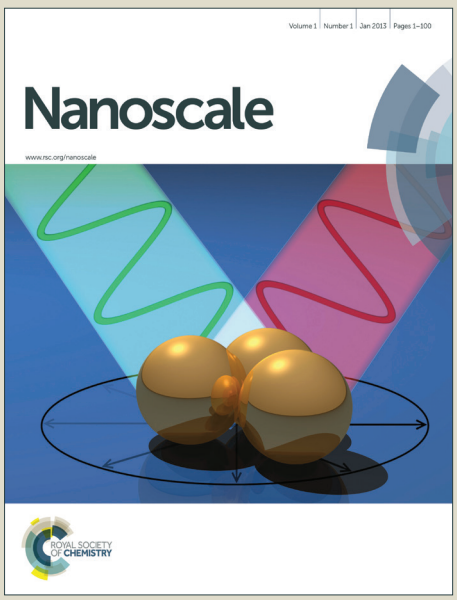

ROYAL SOCIETY OF CHEMISTRY

www.rsc.org/nanoscale

Journal Name

RSCPublishing

ARTICLE

(*n*,*m*) Assignments and Quantification for Single-Walled Carbon Nanotubes on SiO_2/Si Substrates by Resonant Raman Spectroscopy

Cite this: DOI: 10.1039/x0xx00000x

Received 00th January 2012,
Accepted 00th January 2012

DOI: 10.1039/x0xx00000x

www.rsc.org/

Daqi Zhang, Juan Yang*, Feng Yang, Ruoming Li, Meihui Li, Dong Ji, and Yan Li*

The single-walled carbon nanotubes (SWNTs) on silicon substrates are promising candidate for the next generation electronic and photoelectronic devices, therefore, an easy, convenient, and nondestructive method for characterizing such samples is quite important and strongly needed. In this work, we provide in details such a method to assign (*n*,*m*) with considerable accuracy through resonant Raman spectra. We develop an equation of $\omega_{RBM} = 235.9 / d_t + 5.5$ for SWNTs grown by Ni, Co, and Fe catalysts on SiO_2/Si substrates in the d_t range of 1.2-2.1 nm. This method is further utilized to make (*n*,*m*) assignments and quantification for our SWNTs catalyzed by W_6Co_7, which is highly enriched with (12,6). The less abundant chiralities in the samples are also assigned and the contents are analyzed using a counting-based method. Moreover, these chirality-specified samples allow us to collect 1330 RBM data for the single chirality (12,6) and the RBM variation is found no larger than ± 2.5 cm^{-1}. A step-by-step procedure is also provided as a general guide for (*n*,*m*) assignments.

1 Introduction

Single-walled carbon nanotubes (SWNTs) are direct bandgap semiconductors with clear interface and very high electron and hole mobilities.[1] The excellent electronic properties of SWNTs make them good candidates with broad application prospects in the field of nanoelectronic devices.[2,3] In 2013, the first carbon nanotube computer was build.[4] Very recently, IBM has announced that commercial nanotube transistors should be ready around 2020.[5] In order to obtain high performance SWNT-based devices, the preparation of structurally pure SWNT materials, which have uniform chirality (*n*,*m*) and bandgap, has proved to be a critical challenge over the last two decades. Recently, two independent works using either high melting point low symmetry W_6Co_7 catalysts[6] or polycyclic aromatic hydrocarbon precursors[7] provide possible solutions for chirality controllable growth of SWNTs. For analyzing the (*n*,*m*) distribution and for improving the chirality selectivity, apparently, an easy, convenient, and nondestructive method for characterizing the (*n*,*m*) of SWNTs on standard silicon substrates for devices is strongly needed.

The methods widely utilized for (*n*,*m*) characterizations comprise electron diffraction (ED)[8,9] and spectroscopic methods[10] including absorption, photoluminescence (PL), Rayleigh and Raman scattering spectroscopies. However, ED and Rayleigh scattering spectroscopy require suspended samples, and thus are not applicable for SWNTs on substrates. Absorption spectroscopy is widely used for bulk SWNT samples, but normally cannot obtain signals from SWNTs on substrates. Recently, the optical spectra of SWNTs on substrate are obtained using a polarization-based technique, in which a relatively long and straight segment of clean SWNT is needed.[11] PL applies only for semiconducting (S)-SWNTs but not for metallic (M)-SWNTs, and its application for SWNTs on silicon substrates is largely limited due to the quenching of PL on substrates as well as the strong fluorescence background of silicon itself. Resonant Raman (RR) spectroscopy, on the other hand, is a nondestructive, convenient, and low equipment cost method that can be readily utilized for characterization of SWNTs on substrates for both M- and S-SWNTs.

In RR spectroscopy, the (*n*,*m*) of SWNTs are assigned based on

both the electronic transition energies (E_{ii}) provided through the resonance conditions and the tube diameter (d_t) obtained from some diameter-dependent Raman active modes, such as the radial breathing mode (RBM). A relation of $\omega_{RBM} = A / d_t + B$ is established to describe the diameter dependence of RBM frequency.[12,13] The parameter A is determined by the vibrational force constant and the parameter B is associated with the environmental effects,[13] which accounts for tube bundling, substrate-tube interactions, molecules adsorbed onto the tubes, static pressure difference, etc. The value of B is expected to be zero for suspended SWNTs in vacuum. When a SWNT is affected by the environments, the van der Waals interaction-induced pressure will mix into the harmonic oscillator equation. Consequently, A value will be affected and the parameter B will become positive. In 2001, values of A = 248 nm·cm^{-1} and B = 0 was reported for SWNTs on SiO_2/Si substrates.[12] Later, many other ω_{RBM}-d_t relations were reported, including relations for vertically aligned SWNT forests on silicon and quartz substrates,[13] suspended SWNTs,[14,15] surfactant-dispersed SWNTs,[16] etc. Based on these further studies, it is realized that imposing B = 0 for SWNTs on SiO_2/Si substrates is not suitable due to the nonnegligible SWNT-substrate interactions. Moreover, the E_{ii} values were calculated using nearest neighbor tight binding (TB) theory, which did not consider nanotube curvature effects and the exciton effects, leading to some inaccuracy in E_{ii} and inappropriate assignments for small diameter tubes.[13]

In this work, we describe in details an easy and convenient method to make (n,m) assignments with considerable accuracy through RR spectra. We analyze the RR spectra of SWNTs grown on SiO_2/Si substrates by Ni, Co, and Fe catalysts, and an equation between ω_{RBM} and d_t is provided. This method is further utilized to make (n,m) assignments and quantification for our SWNTs catalyzed by W_6Co_7.[6] A step-by-step procedure is also provided as a general guide for (n,m) assignments.

2 Experimental

2.1 Sample Preparation

The random SWNTs were grown by a catalytic chemical vapor deposition (CCVD) method.[17] Ni, Co, Fe, and W_6Co_7 were used as catalysts to prepare random SWNT samples on SiO_2/Si wafers with a thermally grown 300 nm thick SiO_2 layer. For Ni, Fe, and W_6Co_7 catalysts ethanol served as carbon source, and for Co catalyst methane is used as carbon source.

2.2 SEM Characterization

The scanning electron microscopy (SEM) images of SWNTs were taken on a cold field emission scanning microscope (Hitachi S4800) operated at an acceleration voltage of 1.0 kV.

2.3 Raman Characterization

RR spectra of SWNTs were collected with three Horiba Jobin Yvon LabRAM systems, including an ARAMIS spectrometer for 532, 633, and 785 nm laser excitations, a HR800 spectrometer for 488 nm, and another HR800 for 514 and 830 nm laser excitations. These six wavelengths approximately cover 85% of all the chiralities.[6,18] A 100× air objective was used, and the laser spot was about 1 μm in diameter. The laser power was carefully controlled to avoid any heating effect on Raman shifts. An 1800 grooves/mm grating was used, giving a spectral resolution of about 0.7 cm^{-1}. The Raman shifts were calibrated using the peak centered at 520.7 cm^{-1} arising from the SiO_2/Si substrate.

3 Results and Discussion

To ensure the laser spot of 1 μm diameter will cover only one individual SWNT, the samples with low SWNT density are chosen. Typical SEM images of the tested region show an average density of 2-6 SWNTs/100 μm^2 (Figure 1). Samples grown by Ni, Co, and Fe catalysts show similar density and average length.

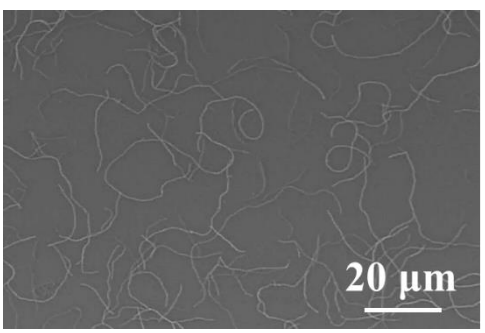

Figure 1. SEM image of a typical sample with random SWNTs on SiO_2/Si substrate catalyzed by Co. The very dilute density of 2-6 SWNTs/100 μm^2 ensures that for each observed RBM signal only one individual SWNT is present under the laser spot of 1 μm in diameter.

3.1 The Reference Kataura Plot

It is well known that not only the ω_{RBM}-d_t relation is highly dependent on environments, but also the E_{ii} values of the same chirality vary from sample to sample and are easily affected by environments.[19,20] Therefore, in order to make proper (n,m) assignments by RR spectroscopy, a reference Kataura plot that is particularly suitable for random SWNTs on SiO_2/Si substrates is

necessary.

Jorio group established systematic equations of E_{ii} as a function of d_t, θ, and i, for vertically aligned "super-growth" SWNT forests on

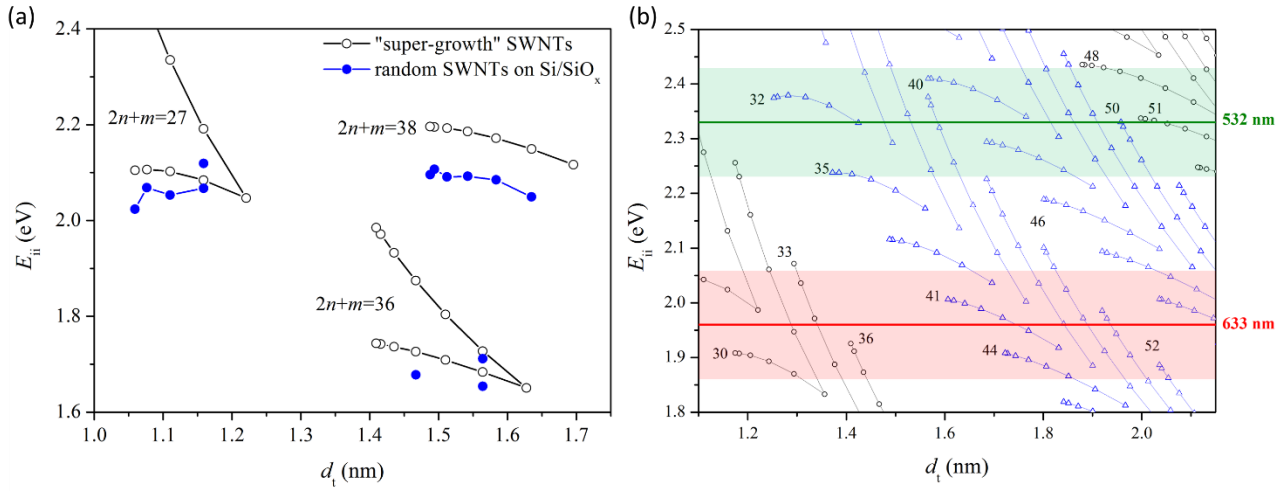

Figure 2. (a) Comparison of the E_{33} for $2n+m$=38 S-SWNTs and E_{11} for $2n+m$=27, 36 M-SWNTs between "super-growth" sample in ref. 20 (black open dots) and random SWNTs on SiO_2/Si substrates in ref. 23 (blue filled dots). (b) The reference Kataura plot used in this work with E_{ii} redshifted by 80 meV for S-SWNTs and 60 meV for M-SWNTs from the reported E_{ii} values of "super-growth" sample in ref. 20. The green and red solid lines indicate the corresponding energies for 532 and 633 nm lasers, respectively. The colored regions over the corresponding laser lines denote the resonance window of ±0.1 eV.

SiO_2/Si substrates.[20-22] Due to the negligible interactions and the well-established equations over a broad range, the E_{ii} values of "super-growth" SWNTs usually serve as standards, from which the E_{ii} values of other SWNT samples can be redshifted.

The magnitude of E_{ii} redshifts is dependent on the SWNT-environment interactions in the samples. For lattice-oriented SWNTs grown on quartz, which is known to have strong interactions with the SWNTs, a 100 meV redshift in E_{ii} from the "super-growth" standards was estimated.[24] For one S-SWNT suspended over trenches on SiO_2/Si substrate, a 55 meV shifts in E_{33} was reported between the supported and suspended parts.[25] A more systematic study[23] on E_{ii} values for random SWNTs on SiO_2/Si substrates obtained the resonant Raman profiles for S-SWNTs in the $2n+m$=38 family and for M-SWNTs in the $2n+m$=27 and 36 families. A comparison between their E_{ii} values and the corresponding "super-growth" standards is illustrated in Figure 2a, resulting in redshifts of 65-100 meV for S-SWNTs and 15-80 meV for M-SWNTs. Therefore, we choose an average redshift of 80 meV for S-SWNTs and 60 meV for M-SWNTs from the reported values of "super-growth" standards for our reference E_{ii} to be used for (n,m) assignments. In the so-obtained reference Kataura plot (Figure 2b), the resonance window of E_{laser} is estimated as ±0.1 eV,[26] indicated by the colored regions over the corresponding laser lines. The uncertainty in d_t is about ±0.01 nm according to both spectral resolution and experimental repeatability, which will be further discussed later.

3.2 Derivation of the ω_{RBM}-d_t Relation

Assignments of SWNTs grown by Ni catalysts

By careful examination of the reference Kataura plot, the region with E_{33} = 2.20 - 2.45 eV and d_t = 1.20 - 1.50 nm (Figure 3a), serves as a good starting point for assignments because only a few semiconducting chiralities are available within this region and all of them are supposed to be in resonance with the 532 nm laser. We denote this particular region as the "sparse region". Random SWNTs on SiO_2/Si substrates all catalyzed by Ni are first examined. The RR spectra (Figure 3b) of four individual SWNTs with ω_{RBM} in the range of 170-190 cm^{-1} are obtained with 532 nm laser excitation. These four SWNTs, labeled as **SWNT-1** to **SWNT-4** from smallest to largest in d_t, are valid (n,m) candidates in the "sparse region". The narrow and non-BWF shape G^- band is known as characteristics of S-SWNTs.[27]

Based on all available ω_{RBM}-d_t relations reported in literatures,[13,20] the largest possible d_t range for **SWNT-1** with ω_{RBM} at 189.3 cm^{-1} is 1.20-1.31 nm, the lower and upper limits of which are calculated from ω_{RBM} = 227 / d_t [13] and ω_{RBM} = 248 / d_t,[12] respectively. **SWNT-2** with ω_{RBM} at 179.1 cm^{-1} is in the d_t range of 1.27-1.39 nm, which is about 0.07-0.08 nm larger than that of

SWNT-1. Clearly, the only two possible candidate pairs in the "sparse region" are: (15,2) & (13,6), and (14,4) & (12,8), for **SWNT-1** & **SWNT-2**, respectively. Although d_t of (16,0) is very close to that of (15,2) and is about 0.07 nm smaller than that of (13,6), it is excluded because the G band of **SWNT-1** does not match a single symmetric Lorentzian band shape expected for zigzag S-SWNTs.[14] d_t of **SWNT-3** with ω_{RBM} at 176.1 cm^{-1} is then calculated to be about 0.02 nm larger than that of **SWNT-2**, which distinctly excludes the (15,2) & (13,6) pair because no possible chirality is available for **SWNT-3** in this case. For the (14,4) & (12,8) pair, (16,3) in the $2n+m$=35 family is a perfect match for **SWNT-3**. Consequently, **SWNT-4** with ω_{RBM} at 170.4 cm^{-1} and d_t about 0.04 nm larger than that of **SWNT-3** can be assigned to (11,10). Based on the assignments for the above four SWNTs in the "sparse region", a tentative function of $\omega_{RBM} = 237.9 / d_t + 4.1$ can be derived.

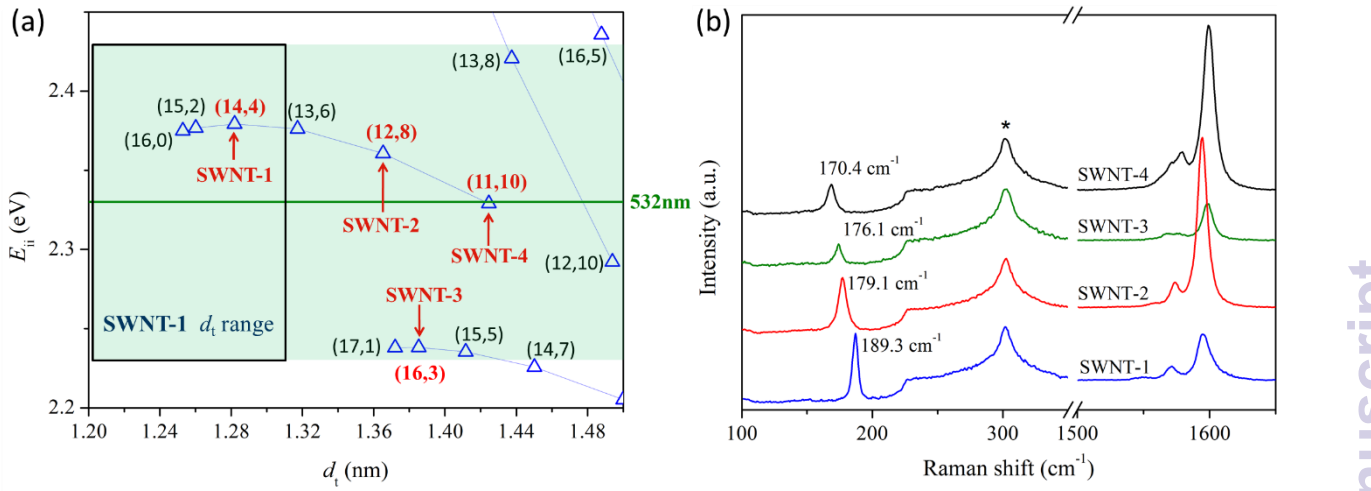

Figure 3. (a) The "sparse region" Kataura plot in the range of E_{33}=2.20-2.45 eV and d_t=1.20-1.50 nm with (n,m) labeled. The black rectangle shows the possible d_t range of SWNT-1. (b) The resonant Raman spectra of four individual SWNTs labeled as SWNT-1 to SWNT-4, the (n,m) assignments of which are given in (a). Peaks indicated by * arise from SiO_2/Si substrates.

Using the tentative ω_{RBM}-d_t relation, all observed ω_{RBM} values for random SWNTs on SiO_2/Si substrates catalyzed by Ni can be calculated as d_t values and plotted onto the reference Kataura plot with respect to the corresponding E_{laser}, shown as black dots in Figure S1a. As Kataura plot contains congested chiralities in many regions which complicates the assignments, even with the calculated d_t as well as the resonance conditions many data points may still lead to ambiguous (n,m) assignments. Fortunately, there are some data points that can be confidently assigned to certain chiralities, indicated by arrows or dashed circles in Figure S1a. For those chiralities, either only one specific (n,m) is available within the uncertainty region of both d_t and E_{ii}, or some supplementary spectroscopic characteristics further support the assignments.

For example, three SWNTs (two with identical ω_{RBM} at 125.4 cm^{-1} and the other with ω_{RBM} at 123.7 cm^{-1}, all excited by 532 nm laser) are observed within an enlarged region shown in Figure S1b, which contains both S- and M-SWNTs. G band shape of these three SWNTs (Figure S1c) can clearly distinguish their S or M nature: **SWNT-5** with ω_{RBM} at 123.7 cm^{-1} shows large BWF shape G$^-$ band and is distinctly an M-type, and thus can be assigned to either (25,1) or (19,10) with identical d_t; the two SWNTs with identical ω_{RBM} at 125.4 cm^{-1} show obviously different G band shape, **SWNT-6** with little G$^+$ and large BWF shape G$^-$ corresponding to an M-SWNT and **SWNT-7** with large G$^+$ component corresponding to an S-SWNT. The assignments can thus be made as (20,8) and (24,2), respectively.

Assignments of SWNTs grown by Co and Fe catalysts

RR spectra of random SWNTs catalyzed by Co and Fe are collected in a similar manner, and the corresponding data points are plotted in Figure S2. As can be seen, by utilizing the tentative ω_{RBM}-d_t relation obtained above, almost all data points are within the uncertainty region of at least one chirality, except for the two SWNTs (both showing semiconducting G band shape) excited by 633 nm laser with d_t in the range of 1.4-1.6 nm. No chirality is available within the ±0.1 eV resonance window for these two data points. We believe these two SWNTs can be assigned to the $2n+m$=38 family. The observation of these two SWNTs slightly out of the ±0.1 eV resonance window might arise from a strong electron-phonon coupling for SWNTs with small chiral angle.[28,29]

To make proper assignments for SWNTs catalyzed by Co and

Fe, further verifications of the (*n*,*m*) are strongly needed. By careful experiments and analysis, we find that the chiralities of two SWNTs, denoted as **SWNT-8** and **9**, can be confirmed by some structure-dependent features, as discussed below:

The RR spectra of **SWNT-8** with 532 nm excitation is shown in Figure S2b. The ω_{RBM} is observed at 157.2 cm^{-1}, corresponding to a d_t value of ~1.55 nm. Only S-SWNTs are available in this E_{ii}-d_t region. The G band of **SWNT-8** presents a nearly perfect single-component, symmetric Lorentzian band shape centered at 1583 cm^{-1} with a FWHM of 5 cm^{-1}. Such symmetric G band feature is characteristics of either zigzag S-SWNTs or armchair M-SWNTs.[14,30-32] Therefore, **SWNT-8** can be assigned to the semiconducting zigzag chirality (20,0).

Figure S2c plots the RR spectra of **SWNT-9** with 633 nm excitation. The ω_{RBM} is observed at 185.3 cm^{-1}, corresponding to a d_t value of ~1.31 nm. In the spectral region of 600-900 cm^{-1}, some weak intermediate frequency mode (IFM) features are clearly observed. The IFM features are reported to be present only in SWNTs with chiral angle $\theta \rightarrow 0$ due to the linear momentum conservation requirement.[33] Therefore, **SWNT-9** can be assigned to the metallic chirality (15,3) with $\theta = 8.9^o$.

For the above two SWNTs catalyzed by Co or Fe, it is found that the calculated d_t values using the tentative ω_{RBM}-d_t relation derived from Ni-catalyzed SWNTs match quite nicely with the d_t values of the corresponding assigned chiralities, suggesting no significant catalyst-specified effects on the ω_{RBM}-d_t relation. Therefore, data of SWNTs catalyzed by Ni, Co, and Fe can be used indiscriminately for the final fitting.

Fitting the Data

For the final fitting, 28 data points with confident assignments are included, and the resultant best fitting equation is $\omega_{RBM} = (235.9 \pm 1.4) / d_t + (5.5 \pm 0.9)$ (Figure 4), only slightly different from the tentative relation derived from four SWNTs in the "sparse region". The corresponding data of the 28 chiralities included in the fitting are summarized in Table 1. The fit is excellent with an $R^2 = 0.9991$, and the average $|\Delta d_t|$, which is the absolute value of the difference between the calculated d_t from the best fitting function and the actual d_t, is only 0.006 nm. Since all measurements are performed in air at room temperature, we believe this relation gives the best fit for random SWNTs on SiO_2/Si substrates in air at room temperature, and is suitable for SWNTs catalyzed by various metal catalysts. According to the available data, this relation suits for SWNTs with d_t in the range of 1.2-2.1 nm.

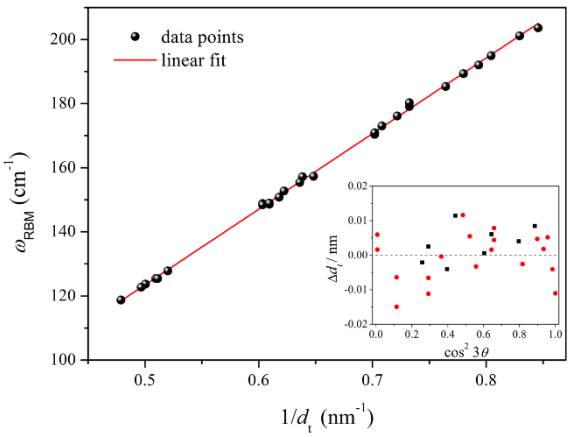

Figure 4. Linear fit of ω_{RBM} with respect to $1/d_t$ for random SWNTs on SiO_2/Si substrates catalyzed by Ni, Co, and Fe. The fitting line gives $\omega_{RBM} = (235.9 \pm 1.4) / d_t + (5.5 \pm 0.9)$ with an $R^2 = 0.9991$, and shows no significant catalyst-specified effects. Inset: difference between calculated d_t from $d_t = 235.9 / (\omega_{RBM} - 5.5)$ and the d_t of tubes with respect to $\cos^2 3\theta$ for both S- (red dots) and M-SWNTs (black squares).

3.3 Assignments and Quantification of SWNTs Grown by W_6Co_7 Catalysts

Assignments of SWNTs Grown by W_6Co_7 Catalysts

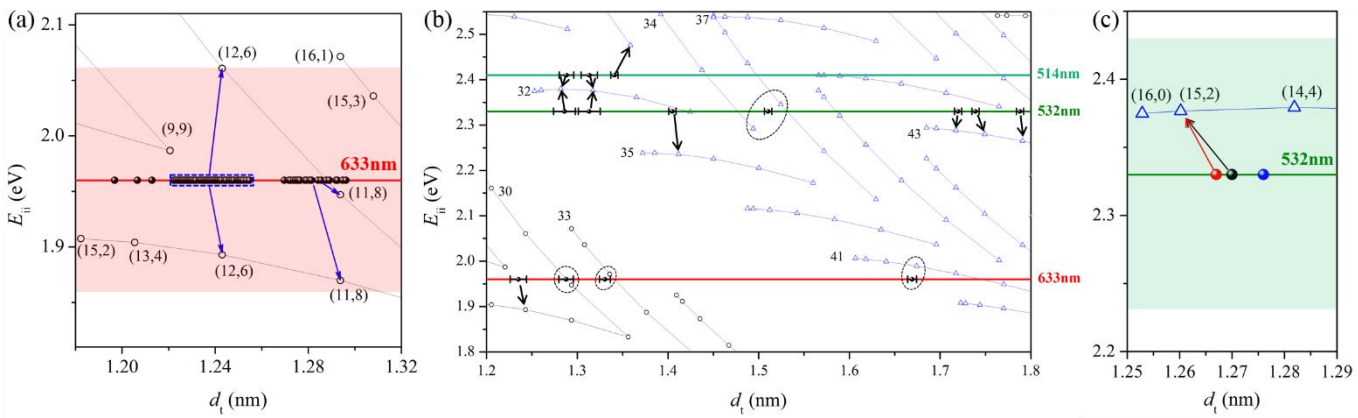

Figure 5. (a) The enlarged Kataura plot showing 1330 RBMs in the range of 193.5-198.5 cm^{-1} assigned to (12,6) and 40 RBMs assigned to (11,8). (b) The Kataura plot with observed RBMs and their (*n*,*m*) assignments for the chirality-specified SWNTs catalyzed by W_6Co_7. Only chiralities with contents higher than 0.1% are shown. (c) The comparison of d_t = 1.267 nm calculated from $\omega_{RBM} = 235.9 / d_t + 5.5$ (red), 1.270 nm from $\omega_{RBM} = 240.5 / d_t + 2.3$ (black), and 1.276 nm from $\omega_{RBM} = 248 / d_t$ (blue, taking in account $a_{C\text{-}C}$ = 0.144 nm) for an observed RBM at 191.7 cm^{-1} and the corresponding assignments.

For our random SWNTs on SiO_2/Si substrates catalyzed by W_6Co_7 reported previously,[6] RBM signal intensely concentrated in the range of 193.5-198.5 cm^{-1} (Figure 5a) is observed under 633 nm laser excitation, whereas other RBM frequencies are only observed very occasionally under all other five laser excitations (488, 514, 532, 785, and 830 nm). The statistical data of RBM suggest a highly chirality-specific growth of SWNTs.

For RBM signals concentrated in the range of 193.5-198.5 cm^{-1} under 633 nm laser excitation, the diameters are calculated to be in the range of 1.222-1.255 nm based on the above ω_{RBM}-d_t relation. Only two chiralities are possible candidates: (12,6) with d_t = 1.243 nm and (9,9) with d_t = 1.221 nm. (9,9) is excluded because it is an armchair tube and the G band should give a symmetric Lorentzian shape, whereas the G band of those SWNTs all show obvious BWF feature.[6] Therefore, the enriched chirality in the sample is assigned unambiguously to (12,6). The ED characterization further confirms this assignment.[6]

Similar assignment procedures are performed for all the other chiralities in the (12,6)-enriched SWNT samples catalyzed by W_6Co_7 . By using the derived ω_{RBM}-d_t relation and the excitation laser energy, as well as verifying by the G band features, we obtain the assignments for almost all observed RBMs. Table 2 summarizes various chiralities with contents higher than 0.04% in the sample. An average difference between the calculated d_t and the d_t of nanotubes is only 0.007 nm for the 21 chiralities listed in Table 2. The assignments for all chiralities with contents higher than 0.1% are shown in Figure 5b and explained as follows: The three chiralities of (11,8), (14,5), and (17,7) excited by 633 nm laser can be assigned unambiguously. Their RBM frequencies were largely separated and no other chirality is present to interfere the assignments. The tubes assigned to (13,6) and (14,4) are double confirmed by the fact that they can be excited by both 514 and 532 nm lasers. The tubes assigned to (11,9) might be ambiguously assigned to the nearby chiralities (13,6) or (12,8). However, it would be expected that these tubes should be excited by both 514 and 532 nm lasers if they were (13,6) or (12,8). The fact that those tubes only appeared under 514 nm but not 532 nm laser excitation verifies the assignment of (11,9). The tubes assigned to (15,5) are not assigned to nearby (11,10) because the difference in diameter would be about 0.020 nm otherwise, which is much larger than the average diameter difference of 0.007 nm for all assigned chiralities. The three chiralities of (19,5), (18,7) and (17,9) excited by 532 nm laser match nicely with three consecutive chiralities in the $2n+m$=43 family and are thus properly assigned. The only ambiguous assignment for chiralities with content higher than 0.1% is (12,10)/(15,7).

Comparing to the previous equation of $\omega_{RBM} = 248 / d_t$ for random SWNTs on SiO_2/Si substrates,[12] our equation of $\omega_{RBM} = 235.9 / d_t + 5.5$ takes the environmental effects into account by the addition of an environmental parameter *B*. Comparing to the previous equation of $\omega_{RBM} = 227 / d_t$ for suspended SWNTs free of interaction with $B = 0$,[13] and the equation of $\omega_{RBM} = 217.8 / d_t + 15.7$ for SWNTs on quartz with substantial substrate-tube interactions,[34] our equation gives a moderate *B* value of 5.5 cm^{-1}, in good accordance to the mild substrate-tube interactions for SWNTs on SiO_2/Si substrates.

Moreover, the relation obtained in this work only differ slightly in the d_t range of 1.2-2.1 nm from our previous relation of $\omega_{RBM} = 240.5 / d_t + 2.3$ used to assign (12,6)-enriched samples.[6] This similarity shows that the present relation can be further applied to assign SWNTs grown on SiO_2/Si substrates by other catalysts.

As an example to show how different assignments can be made with different equations, Figure 5c plots the calculated d_t values of 1.267 nm from the present relation $\omega_{RBM} = 235.9 / d_t + 5.5$ (red), 1.270 nm from $\omega_{RBM} = 240.5 / d_t + 2.3$ (black), and 1.276 nm from $\omega_{RBM} = 248 / d_t$ (blue, taking into account $a_{C\text{-}C}$ = 0.144 nm), respectively, for an observed RBM at 191.7 cm^{-1}. Both red and black datapoints give an assignment of (15,2) but the blue datapoint will lead to an assignment of (14,4). Since (15,2) and (14,4) are chiralities in the "sparse region", we are very sure that this RBM corresponds to a (15,2) tube.

Quantification of SWNTs Grown by W_6Co_7 Catalysts

For quantification of the (*n*,*m*) contents in the sample, we use altogether 1863 RBM data under six different lasers in the statistics, taking into careful account for the fact that some specific chiralities might be excited by both 514 and 532 nm lasers. Note that the same area of SWNT samples is scanned in a similar manner for all six lasers. 1330 out of 1863 RBM data are assigned to (12,6). Typically

5-9 tubes are observed in the laser spot of 1 μm diameter. An average of 6.7 tubes is calculated from 7 samples based on SEM images (e.g. Figure S4). It is apparent that only one RBM peak will appear even multiple (12,6) tubes are present within the laser spot. Considering the factor that the six lasers we used cover ~85% of all SWNT chiralities,[6,18] the calibrated content of (12,6) can be estimated from the equation:

$$x_{(12,6)} = \frac{N_{(12,6)} \cdot \bar{n} \cdot x_{(12,6)}}{N_{(12,6)} \cdot \bar{n} \cdot x_{(12,6)} + N_{\text{others}}/0.85}, \quad \text{(Eq. 1)}$$

where $x_{(12,6)}$ is the calibrated content of (12,6) in the sample, $N_{(12,6)}$ is the total times that RBM for (12,6) is observed, N_{others} is the total times that RBM for all other chiralities is observed, and $\bar{n}$ is the average number of SWNTs under the laser spot. The calibrated content of (12,6) is then calculated to be 93.0% using $\bar{n}$ = 6.7, in good accordance with the abundance of 92.5% obtained from the absorption spectra.[6] Notably, although the value of $\bar{n}$ might not be very accurate, however, calculations show that even a relative error of ±20% in $\bar{n}$ will only cause less than 2% error in $x_{(12,6)}$.

The calibrated content of other excited chiralities can be estimated from the equation:

$$x_{(n,m)} = \frac{N_{(n,m)}}{N_{(12,6)} \cdot \bar{n} \cdot x_{(12,6)} + N_{\text{others}}/0.85}, \quad \text{(Eq. 2)}$$

where $x_{(n,m)}$ is the calibrated content of a certain excited (n,m) other than (12,6), and $N_{(n,m)}$ is the total times that RBM for this (n,m) is observed. The total calibrated content of the chiralities that are not excited by all six lasers can be estimated from the equation:

$$\sum_{(n,m)} x'_{(n,m)} = \frac{N_{\text{others}} \times 0.15/0.85}{N_{(12,6)} \cdot \bar{n} \cdot x_{(12,6)} + N_{\text{others}}/0.85} \quad \text{(Eq. 3)}$$

Clearly,

$$x_{(12,6)} + \sum_{(n,m)} x_{(n,m)} + \sum_{(n,m)} x'_{(n,m)} = 1.$$

Meanwhile, our chirality-specified samples also make it possible for us to obtain some useful experimental information for one single chirality. All 1330 RBM for (12,6) are observed in the range of 193.5-198.5 cm^{-1}. The statistical data give an average ω_{RBM} of 196.5 cm^{-1} with a standard deviation of 1.3 cm^{-1}. After converting into d_t, the corresponding values are 1.235 ± 0.009 nm. The RBM variations for all other chiralities in the samples are indeed less than ± 2.5 cm^{-1}. Therefore, we believe that the possible RBM range for any single (n,m) based on RR spectroscopy should be no larger than ± 2.5 cm^{-1}, and that ± 0.01 nm is a good estimation as the uncertainty in d_t due to data repeatability. We also believe that the ±2.5 cm^{-1} variance of RBM frequency for a single chirality should cover the influence of all experimental condition factors, including routine differences in humidity, temperature, storage conditions, oxide thickness, etc.

3.4 Procedure for (n,m) Assignments

As is stated above, we show in details the establishment of the ω_{RBM}-d_t relation for a particular SWNT sample and the (n,m) assignments with RR spectroscopy. In brief, the procedure for (n,m) assignments can be summarized as follows:

1. Obtain the reference Kataura plot with suitable E_{ii} values for the particular SWNT sample. The E_{ii} values may be shifted by a reasonable magnitude from certain SWNT standards.[34,35]
2. Obtain a suitable ω_{RBM}-d_t relation for the particular SWNT sample. For example, choose a certain "sparse region" to start with, derive a tentative relation from several SWNTs in this region, and determine the best fit equation with more data. You may use some structure-dependent features and other supplementary techniques to verify your assignments.
3. Assign the (n,m) of SWNTs by the experimental ω_{RBM} obtained with RR spectroscopy:
   1) Convert the experimental ω_{RBM} into d_t by applying the ω_{RBM}-d_t relation. Mark all converted data points with corresponding E_{laser} on the reference Kataura plot. Determine the groups of data points that should be assigned to the same (n,m). Notably, the ω_{RBM} range for the same (n,m) should be no larger than ±2.5 cm^{-1}. Calculate the average d_t and the standard deviation for each group of data points.
   2) Determine the uncertainty region for each group of data points. Normally, the resonance window of E_{laser} is about ±0.1 eV.[26] For (n,m) with small θ, the resonance window might be slightly larger due to a strong electron-phonon coupling.[28] The uncertainty in d_t can be estimated according to both spectral resolution and experimental repeatability, and is usually in the order of ±0.01 nm.
   3) Assign the group of data points to certain (n,m) in the uncertainty region. If only one (n,m) is available in the corresponding uncertainty region, the assignment can be made unambiguously. If more than one (n,m) are available, supplementary information needs to take into account. For example, the G band shape and frequency,[14,32,36,37] IFM

features,[33] simultaneous excitation under multiple laser lines, etc.

4 Conclusions

In this work, we obtain a reference Kataura plot that is suitable for SWNTs on SiO_2/Si substrates by redshifting E_{ii} by 80 meV for S-SWNTs and 60 meV for M-SWNTs from the reported values of "super-growth" SWNTs. We obtain an equation of $\omega_{RBM} = 235.9 / d_t + 5.5$ for SWNTs in the d_t range of 1.2-2.1 nm on SiO_2/Si substrates catalyzed by various metal catalysts. No significant catalyst-specified effect is observed on this relation. Using this derived ω_{RBM}-d_t relation, the chirality-specified SWNT sample catalyzed by W_6Co_7 is properly assigned and quantified. A (12,6) content of 93.0% is calculated based on 1863 RBM statistical data under six different lasers, which is in good agreement with the abundance of 92.5% obtained from the absorption spectra. An average difference of 0.007 nm between the calculated d_t and the d_t of nanotubes for all 21 assigned chiralities indicate the good assignments. Moreover, our chirality-specified samples provide us an opportunity to investigate the possible RBM variations of a single chirality. Based on the maximum variation of ±2.5 cm^{-1} for 1330 statistics RBM data of (12,6), we conclude that the RBM variation for a single chirality should be no larger than ±2.5 cm^{-1}.

Acknowledgment

The authors would like to thank Prof. K. Jiang and Prof. S. Wang for Raman measurements. This research was financially supported by NSFC (Projects 21125103 and 91333105), MOST (Project 2011CB933003), Beijing Higher Education Young Elite Teacher Project (No. YETP0007), Beijing Municipal Science & Technology Commission (No. D141100000614001) for support.

Notes and references

[a] Address here. Beijing National Laboratory for Molecular Sciences, Key Laboratory for the Physics and Chemistry of Nanodevices, State Key Laboratory of Rare Earth Materials Chemistry and Applications, College of Chemistry and Molecular Engineering, Peking University, Beijing 100871, China.
Email: yang_juan@pku.edu.cn, yanli@pku.edu.cn.

Electronic Supplementary Information (ESI) available: Supplementary Figures S1-S4. See DOI: 10.1039/b000000x/

1. R. Saito, G. Dresselhaus and M. S. Dresselhaus, *Physical properties of carbon nanotubes*, World Scientific, 1998.
2. P. L. McEuen, *Nature*, 1998, **393**, 15-17.
3. P. Avouris, Z. Chen and V. Perebeinos, *Nat Nanotech*, 2007, **2**, 605-615.
4. M. M. Shulaker, G. Hills, N. Patil, H. Wei, H.-Y. Chen, H.-S. P. Wong and S. Mitra, *Nature*, 2013, **501**, 526-530.
5. http://www-03.ibm.com/press/us/en/pressrelease/44357.wss.
6. F. Yang, X. Wang, D. Zhang, J. Yang, LuoDa, Z. Xu, J. Wei, J.-Q. Wang, Z. Xu, F. Peng, X. Li, R. Li, Y. Li, M. Li, X. Bai, F. Ding and Y. Li, *Nature*, 2014, **510**, 522-524.
7. J. R. Sanchez-Valencia, T. Dienel, O. Gröning, I. Shorubalko, A. Mueller, M. Jansen, K. Amsharov, P. Ruffieux and R. Fasel, *Nature*, 2014, **512**, 61-64.
8. M. Gao, J. Zuo, R. Twesten, I. Petrov, L. Nagahara and R. Zhang, *Appl Phys Lett*, 2003, **82**, 2703-2705.
9. H. Jiang, A. G. Nasibulin, D. P. Brown and E. I. Kauppinen, *Carbon*, 2007, **45**, 662-667.
10. D. Zhang, J. Yang and Y. Li, *Small*, 2013, **9**, 1284-1304.
11. K. Liu, X. Hong, Q. Zhou, C. Jin, J. Li, W. Zhou, J. Liu, E. Wang, A. Zettl and F. Wang, *Nat Nanotech*, 2013, **8**, 917-922.
12. A. Jorio, R. Saito, J. H. Hafner, C. M. Lieber, M. Hunter, T. McClure, G. Dresselhaus and M. S. Dresselhaus, *Phys Rev Lett*, 2001, **86**, 1118-1121.
13. P. Araujo, I. Maciel, P. Pesce, M. Pimenta, S. Doorn, H. Qian, A. Hartschuh, M. Steiner, L. Grigorian, K. Hata and A. Jorio, *Phys Rev B*, 2008, **77**, 241403.
14. T. Michel, M. Paillet, D. Nakabayashi, M. Picher, V. Jourdain, J. Meyer, A. A. Zahab and J. L. Sauvajol, *Phys Rev B*, 2009, **80**, 245416.
15. K. Liu, W. Wang, M. Wu, F. Xiao, X. Hong, S. Aloni, X. Bai, E. Wang and F. Wang, *Phys Rev B*, 2011, **83**, 113404.
16. C. Fantini, A. Jorio, M. Souza, M. Strano, M. Dresselhaus and M. Pimenta, *Phys Rev Lett*, 2004, **93**, 147406.
17. L. Ding, W. Zhou, H. Chu, Z. Jin, Y. Zhang and Y. Li, *Chem Mater*, 2006, **18**, 4109-4114.
18. M. Fouquet, B. Bayer, S. Esconjauregui, R. Blume, J. Warner, S. Hofmann, R. Schlögl, C. Thomsen and J. Robertson, *Phys Rev B*, 2012, **85**, 235411.
19. J. Lefebvre, J. Fraser, Y. Homma and P. Finnie, *Appl Phys A*, 2004, **78**, 1107-1110.
20. P. Araujo, P. Pesce, M. Dresselhaus, K. Sato, R. Saito and A. Jorio, *Physica E: Low-dimensional Systems and Nanostructures*, 2010, **42**, 1251-1261.
21. S. K. Doorn, P. T. Araujo, K. Hata and A. Jorio, *Phys Rev B*, 2008, **78**, 165408.
22. P. Araujo and A. Jorio, *physica status solidi (b)*, 2008, **245**, 2201-2204.
23. Y. P. Hsieh, M. Hofmann, H. Farhat, E. B. Barros, M. Kalbac, J. Kong, C. T. Liang, Y. F. Chen and M. S. Dresselhaus, *Appl Phys Lett*, 2010, **96**, 103118
24. J. S. Soares, L. G. Cançado, E. B. Barros and A. Jorio, *physica status solidi (b)*, 2010, **247**, 2835-2837.
25. M. Steiner, M. Freitag, J. C. Tsang, V. Perebeinos, A. A. Bol, A. V. Failla and P. Avouris, *Appl Phys A*, 2009, **96**, 271-282.
26. A. Souza Filho, A. Jorio, A. K. Swan, M. Ünlü, B. Goldberg, R. Saito, J. Hafner, C. Lieber, M. Pimenta and G. Dresselhaus, *Phys Rev B*, 2002, **65**, 085417.
27. A. Jorio, A. Souza Filho, G. Dresselhaus, M. Dresselhaus, A. Swan, M. Ünlü, B. Goldberg, M. Pimenta, J. Hafner and C. Lieber, *Phys Rev B*, 2002, **65**, 155412.
28. P. Pesce, P. Araujo, P. Nikolaev, S. Doorn, K. Hata, R. Saito, M. Dresselhaus and A. Jorio, *Appl Phys Lett*, 2010, **96**, 051910.
29. H. Telg, J. Maultzsch, S. Reich, F. Hennrich and C. Thomsen, *Phys Rev Lett*, 2004, **93**, 177401.

30. T. Michel, M. Paillet, A. Zahab, D. Nakabayashi, V. Jourdain, R. Parret and J. Sauvajol, *Adv Nat Sci: Nanosci Nanotechnol*, 2011, **1**, 045007.
31. C. Voisin, S. Berger, S. Berciaud, H. Yan, J. S. Lauret, G. Cassabois, P. Roussignol, J. Hone and T. F. Heinz, *physica status solidi (b)*, 2012, **249**, 900-906.
32. E. H. Hároz, J. G. Duque, W. D. Rice, C. G. Densmore, J. Kono and S. K. Doorn, *Phys Rev B*, 2011, **84**, 121403.
33. J. Wang, J. Yang, D. Zhang and Y. Li, *J Phys Chem C*, 2012, **116**, 23826-23832.
34. P. T. Araujo, S. K. Doorn, S. Kilina, S. Tretiak, E. Einarsson, S. Maruyama, H. Chacham, M. A. Pimenta and A. Jorio, *Phys Rev Lett*, 2007, **98**, 67401.
35. K. Liu, J. Deslippe, F. Xiao, R. B. Capaz, X. Hong, S. Aloni, A. Zettl, W. Wang, X. Bai, S. G. Louie, E. Wang and F. Wang, *Nat Nanotech*, 2012, **7**, 325.
36. H. Telg, J. G. Duque, M. Staiger, X. Tu, F. Hennrich, M. M. Kappes, M. Zheng, J. Maultzsch, C. Thomsen and S. K. Doorn, *ACS Nano*, 2011, **6**, 904-911.
37. H. Telg, E. H. Hároz, J. G. Duque, X. Tu, C. Y. Khripin, J. A. Fagan, M. Zheng, J. Kono and S. K. Doorn, *Phys Rev B*, 2014, **90**, 245422.

Table 1. (*n*,*m*) assignments of random SWNTs on SiO2/Si substrates catalyzed by Ni, Co, and Fe.

ω_{RBM} (cm^{-1})	Catalysts	E_{Laser} (eV)	Assigned (*n*,*m*)	Metallicity	d_t (nm)	θ	Calc. d_t [a] (nm)	Δd_t [b] (nm)
189.3	Ni	2.33	(14,4)	S	1.282	12.2	1.283	0.001
179.1	Ni	2.33	(12,8)	S	1.365	23.4	1.359	-0.006
176.1	Ni	2.33	(16,3)	S	1.385	8.4	1.383	-0.003
170.4	Ni	2.33	(11,10)	S	1.425	28.4	1.431	0.006
150.8	Ni	2.33	(17,6)	S	1.618	14.6	1.624	0.006
148.8	Ni	2.33	(16,8)	S	1.657	19.1	1.646	-0.011
125.4	Ni	2.33	(24,2)	S	1.962	4.0	1.967	0.005
125.4	Ni	2.33	(20,8)	M	1.956	16.1	1.967	0.011
123.7	Ni	2.33	(25,1) or (19,10)	M	1.998	1.9 or 19.8	1.996	-0.002
203.6	Ni	1.96	(14,2)	M	1.182	6.6	1.191	0.009
201.1	Ni	1.96	(13,4)	M	1.205	13.0	1.206	0.001
152.7	Ni	1.96	(20,1)	S	1.607	2.4	1.603	-0.004
148.6	Ni	1.96	(18,5)	S	1.641	11.9	1.648	0.007
122.7	Ni	1.96	(20,9)	S	2.013	17.6	2.013	0.000
192.0	Co	2.33	(15,2)	S	1.260	6.2	1.265	0.005
170.9	Co	2.33	(11,10)	S	1.425	28.4	1.426	0.001
157.2	Co	2.33	(20,0)	S	1.566	0	1.555	-0.011
155.4	Co	2.33	(19,2)	S	1.572	4.9	1.574	0.002
118.7	Co	2.33	(21,9)	M	2.088	17.0	2.084	-0.004
198.2	Co	1.96	(9,9)	M	1.221	30.0	1.224	0.003
194.9	Co	1.96	(12,6)	M	1.243	19.1	1.246	0.003
185.3	Co	1.96	(15,3)	M	1.308	8.9	1.312	0.004
157.3	Co	1.96	(16,6)	S	1.542	15.3	1.554	0.012
148.9	Co	1.96	(18,5)	S	1.641	11.9	1.645	0.004
180.2	Fe	2.33	(12,8)	S	1.365	23.4	1.350	-0.015
173.0	Fe	2.33	(15,5)	S	1.412	13.9	1.408	-0.004
148.4	Fe	2.33	(16,8)	S	1.657	19.1	1.651	-0.006
127.8	Fe	2.33	(21,6)	M	1.923	12.2	1.929	0.006

[a] Calc. d_t is calculated from ω_{RBM} using $d_t = 235.9 / (\omega_{RBM} - 5.5)$.
[b] Δd_t = Calc. d_t - d_t.

Table 2. Statistics on the RBM peaks and the corresponding (*n*,*m*) for random SWNTs catalyzed by W_6Co_7. The analysis is based on 1863 RBM peaks collected under 488, 514, 532, 633, 785, and 830 nm laser excitations. Components with calibrated contents less than 0.04% are not included individually.

Assigned (*n*,*m*)	d_t (nm)	Calc. d_t [a] (nm)	Δd_t [b] (nm)	Laser (eV)	Times observed	Frequencies of appearance (%)	Calibrated Content (%)
(12,6)	1.243	1.235±0.009	-0.008	1.96	1330	71.4	93.0
(13,6)	1.317	1.313±0.009 1.313±0.012	-0.004 -0.004	2.41 2.33	60	3.2	0.67
(15,5)	1.412	1.405±0.004	-0.007	2.33	56	3.0	0.63
(19,5)	1.717	1.720±0.004	0.003	2.33	42	2.3	0.47
(11,8)	1.294	1.288±0.008	-0.006	1.96	40	2.1	0.45
(17,7)	1.674	1.669±0.005	-0.005	1.96	31	1.7	0.35
(14,5)	1.336	1.331±0.006	-0.005	1.96	29	1.6	0.33
(11,9)	1.359	1.341±0.004	-0.018	2.41	22	1.2	0.25
(12,10)/ (15,7)	1.494/ 1.524	1.511±0.004	0.017/ -0.013	2.33	22	1.2	0.25
(14,4)	1.282	1.288±0.008 1.286±0.012	0.006 0.004	2.41 2.33	13	0.7	0.15
(18,7)	1.749	1.739±0.004	-0.010	2.33	10	0.5	0.11
(17,9)	1.791	1.788±0.004	-0.003	2.33	9	0.5	0.10
(16,3)	1.385	1.388±0.004	0.003	2.33	6	0.3	0.07
(13,8)	1.437	1.446±0.008	0.009	2.33	5	0.3	0.06
(14,12)	1.765	1.766±0.004	0.001	2.33	5	0.3	0.06
(15,11)/ (19,6)	1.770	1.780±0.004	0.010	1.96	5	0.3	0.06
(15,2)	1.260	1.267±0.004	0.007	2.33	5	0.3	0.06
(10,5)	1.036	1.031±0.010	-0.005	1.58	4	0.2	0.04
(14,7)	1.450	1.465±0.005	0.015	2.33	4	0.2	0.04
(16,5)	1.488	1.488±0.010	0	2.54	4	0.2	0.04
(17,6)	1.618	1.625±0.016	0.007	2.33	4	0.2	0.04
Other excited (*n*,*m*)	/	/	/	/	157	8.4	1.76
non-excited (*n*,*m*)	/	/	/	/	(94) [c]	/	1.06

[a] Calc. d_t is calculated from ω_{RBM} using $d_t = 235.9 / (\omega_{RBM} - 5.5)$.
[b] Δd_t = Calc. d_t - d_t.
[c] Calculated from (1863 - 1330)×0.15 / 0.85 = 94.